Polymer 51 (2010) 6258–6267

Contents lists available at ScienceDirect

Polymer

journal homepage: www.elsevier.com/locate/polymer

Membranes with through-thickness porosity prepared by unidirectional freezing

Min Kyung Lee, Nae-Oh Chung, Jonghwi Lee*

Department of Chemical Engineering and Materials Science, Chung-Ang University, 221 Heukseok-dong, Dongjak-gu, Seoul, 156-756, South Korea

ARTICLE INFO

Article history:
Received 6 June 2010
Received in revised form
9 October 2010
Accepted 23 October 2010
Available online 30 October 2010

Keywords:
Directional freezing
Porous film network
Freeze-drying

ABSTRACT

Directional freezing is a simple and environmentally friendly method for producing aligned porous materials. Porous structures of uniaxially aligned nanoparticles can be produced by unidirectional freezing a concentrated nanoparticle dispersion and subsequent freeze-drying. However, mechanically strong through-thickness membranes have seldom been reported. The film prepared by directional freezing and subsequent freeze-drying is usually too weak to be a free-standing membrane. By using precise control of freezing rate and direction, we successfully produced free-standing films (with 20–200 μm thickness and 40–60 vol% through-thickness porosity) from inorganic particles/polymer (polytetrafluoroethylene and polyvinylidene fluoride) composites. The pore size could be conveniently controlled by freezing rate and dispersion concentration. The use of composite materials, emulsion states, and post-annealing processes facilitated the preparation of free-standing two-dimensional particulate networks due to enhanced interparticulate coherence. This method could provide novel porous networks with controlled morphology, reduced tortuosity, and enhanced mechanical properties, which have broad applications such as separation/purification, fuel cells, nanocomposites, catalysts, tissue engineering, controlled delivery, and other medical applications.

1. Introduction

Creating aligned porous materials is important to enhance their performance in potential applications, such as tissue engineering, separation, energy generation, and drug release [1–3]. Such porous materials have been typically fabricated through complex processes, such as thermally induced phase separation (TIPS), electrochemical fabrication, microfabrication, and lithography. The ideal fabrication process has to be not only efficient but also adaptable enough to deal with numerous materials of the desired dimensions.

Directional freezing methods may help overcome the existing limits of conventional processes [4–9]. In this approach, ice crystals are used as a template to produce a porous 2D aligned structure. A solution or colloidal dispersion is directionally frozen and that the ice crystals (or solvent crystals) are unidirectionally aligned. The structures of pores after drying reflect the spaces occupied by the unidirectionally frozen and aligned ice crystals (or solvent crystals). The growing ice crystals expel the nanoparticles (or molecules), and heat transfer from the moving interface of ice-water into the remaining unfrozen water. Under these conditions, the nanoparticles aggregate in the cryo-concentrate phases between the growing ice crystals. The morphology of pores can be tailored by controlling the freezing conditions.

Recently, directional freezing has been investigated for the preparation of controlled lamellar structures of ceramic and polymeric materials [5–13]. Aqueous polymer solutions, colloids, or their mixtures have been aligned to form biomimetic structures for advanced materials. The control of morphology and porosity has been attempted using various methods. Although many advanced porous materials have been investigated with directional freezing, the production of mechanically strong membranes with through-thickness pores still remains a considerable challenge.

Although the unidirectional freezing process is similar to freeze-drying, it differs in that the process controls the movement of the freezing front. The controlled movement of the freezing front allows the creation of well-structured materials with fewer defects. Outstanding mechanical properties have been reported in biomimetic ceramic materials prepared from a unidirectional freezing method [5]. In contrast, in the field of polymers, a freeze-drying process is still difficult to produce mechanically strong free-standing polymeric materials (foams). Layered silicates, carbon or cellulose nanofibers, and metal nanoparticles have been used to strengthen the polymeric foams [14–17]. Freeze-drying has been more often used for the preparation of dispersible nanoparticulate powders of drugs with polymers, which is quite the opposite of a mechanically strong, porous foam [18,19].

* Corresponding author. Tel.: +82 2 816 5269; fax: +82 2 824 3495.
E-mail address: jong@cau.ac.kr (J. Lee).

0032-3861/$ – see front matter © 2010 Elsevier Ltd. All rights reserved.
doi:10.1016/j.polymer.2010.10.037

In this work, we investigated the possibility of through-thickness pore membrane preparation via the columnar pore formation by the directional freezing methods. We focused on how to prepare *free-standing* particulate networks with *through-thickness* pores using poly(vinylidene fluoride) (PVDF) and polytetrafluoroethylene (PTFE) and how to control the columnar pore morphology, tortuosity, interconnectivity, and mechanical properties of the structures using unidirectional freeze-drying. We used various nanoparticles, SiO_2, TiO_2, poly(styrene sulfonate)-poly(3,4-ethylene dioxythiophene) (PSS–PEDOT), and PTFE, along with the polymers, PVDF and hydroxypropyl cellulose (HPC), as structuring agents for the porous networks (matrix).

2. Experimental

2.1. Materials

Aqueous monodisperse nano-dispersions containing 20 nm (average diameter) SiO_2 particles (30 wt%, ENB Korea, Daejeon, Korea), 200 nm PSS–PEDOT particles (1 wt%, Aldrich, St. Louis, MO, USA), and 200 nm PTFE particles (60 wt%, Aldrich, USA) were used as received. HPC ($M_w = 80{,}000$ g/mol) and PVDF ($M_w = 180{,}000$ g/mol) were purchased from Aldrich (USA) and used as received. The desired dispersion concentrations were adjusted by dilution with HPLC-grade water (J.T. Baker, NJ, USA).

2.2. Formation of aligned porous networks of nanoparticles

The experimental setup for directional freezing (Fig. 1) was designed to obtain defect-free films of well-ordered through-thickness pores. The film thickness was controlled to be 20–150 μm by adjusting the amount of sample. Polymeric solutions or nanoparticle dispersions were spread on a glass (or PTFE) substrate (4 × 2 cm), which was moved to a liquid nitrogen reservoir at a controlled freezing rate of 10–200 μm. At a certain distance from the reservoir, freezing started from the bottom and spread to the top of the sample. In this freezing step, a sample was cooled to induce ice crystal growth along the vertical direction. Time for complete freezing was controlled by varying the moving speed of a substrate connected to a syringe pump (KDS 100 model, KdScientific, Holliston, MA, USA). To obtain reproducible results, all other experimental factors, such as the amounts of sample and liquid nitrogen, were carefully kept constant. The frozen sample was then freeze-dried using an FD-1000 freeze dryer (EYELA, Tokyo, Japan, trap chilling temperature −45 °C, 5.6 Pa) for 24 h.

2.3. Formation of aligned networks of inorganic nanoparticles/polymer composites

To prepare aligned porous networks of inorganic nanoparticles/polymer composites, PVDF or HPC was used as a structuring agent (polymer matrix). A mixture of SiO_2 aq. dispersion and PVDF solution in DMSO (dimethyl sulfoxide) was frozen unidirectionally to produce composite materials (SiO_2/PVDF: 120/1 wt ratio). Alternately, a mixture of SiO_2 aq. dispersion and HPC aq. solution was used (SiO_2/HPC: 3/1 wt ratio). Depending on solubility for each polymer/solvent, SiO_2/polymer weight ratio was decided. When the weight ratio of SiO_2/PVDF is below 120/1, precipitation of PVDF was observed.

2.4. Formation of aligned networks by the controlled freezing of emulsion

The controlled freezing method was readily extended to emulsions. An organic solution of PVDF/cyclohexanone was prepared, and a SiO_2 aq. dispersion was dispersed into the solution (SiO_2/PVDF: 6/4 wt ratio). The volume ratio of water/cyclohexanone solutions was kept at 3/7. Water-in-oil emulsions were formed by homogenizing (T8 ULTRA-TURAX Homogenizer, IKA®-WERKE, Staufen, Germany) for 20 min, resulting in droplet sizes of 500 nm to 1 μm (from optical microscopy). The emulsion was spread on a glass (or PTFE) substrate and then frozen to produce an aligned network. The frozen emulsions were kept under a nitrogen atmosphere until they were dried in the FD-1000 freeze dryer.

2.5. Characterizations

Network morphologies were investigated by field emission scanning electron microscopy (FESEM, S-4700, Hitachi, Japan) at an accelerating voltage of 15 kV after coating samples with a platinum layer by ion sputtering (E-1030, Hitachi, Japan). An optical microscope (BX-51, Olympus, Japan) was used to obtain images of entire structures with ice crystals. The number average pore sizes of samples were measured by using Scion Image software (Alpha 4.0.3.2, NIH, MD, USA). Three images from each sample were analyzed to obtain the mean pore size (mean size of their minor axes). The surface mechanical properties of materials were obtained through the analysis of force–distance (F–D) curves generated by atomic force microscopy (AFM, XE-100, Park Systems, South Korea). Prior to the F-D measurement, cantilevers were calibrated using reference cantilevers (CLFC-NOBO, Veeco, Santa Babara, CA, USA) with their known spring constants (k_{ref}), following

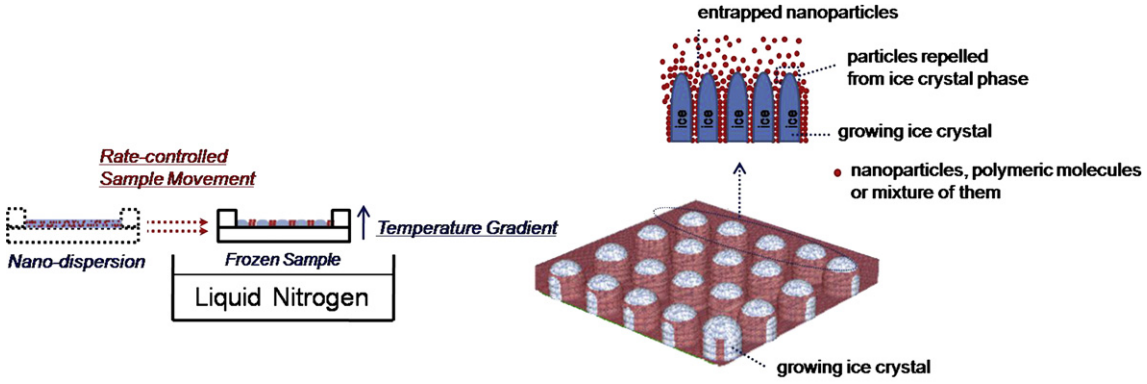

Fig. 1. Schematic representation of the unidirectional freezing method for the preparation of porous networks. The sample moving speed (freezing rate) was controlled to be 10–200 μm/s. The sample was moved toward the liquid nitrogen reservoir to generate columnar ice crystal growth along the vertical direction. The dashed line indicates the direction of sample movement.

a procedure developed by Tortonese and Kirk [20]. The silicon cantilever (NSC15, MikroMasch, Spain) with a spring constant of 30.05 (±3.7) N/m was used for all F–D measurements. The data were acquired at 0.5 μm/s down and up speed. The AFM was operated inside a closed enclosure. For each specimen, 100 repeated measurements were performed at different positions of different samples (temperature: 20 °C, humidity: 25%). ForceView software, written by Janshoff and Oberdoerfer, was used to convert deflection-separation raw data into F–D curves [21]. Using these procedures, the hardness and adhesion force values of the porous networks were obtained [21,22].

3. Results

3.1. Nanoparticulate porous structures

We used a nitrogen reservoir to generate a temperature gradient, similar to our previous experiments in freeze-drying drug nanoparticles [18,19]. Temperature gradient-induced freezing aligned the growth of ice crystals and subsequently the phases of the particles and polymers. After freeze-drying, aligned pores were uniformly formed over the entire sample without noticeable defects. These pores were generated from the sublimation of the aligned columnar ice crystals along the temperature gradient. Typical SEM micrographs of films prepared by unidirectional freezing are shown in Fig. 2.

We first applied the unidirectional freezing technique for various nanoparticles under the conditions designed to create columnar ice crystals. Directional freezing produced well-ordered pore structures in the freezing direction. A cross-sectional image of the aligned through-thickness porous network of SiO_2 nanoparticles is shown in Fig. 2a. The vertical section along the alignment axis (arrow in Fig. 2b) shows the existence of ordered arrays of cylindrical ice domains oriented perpendicular to the substrate. We could control their thickness from 20 to 150 μm.

Long-range arrangement of the pores of the aligned network could be obtained without significant defects, as can be seen in Fig. 2c, which shows a network of PTFE particles. The magnified

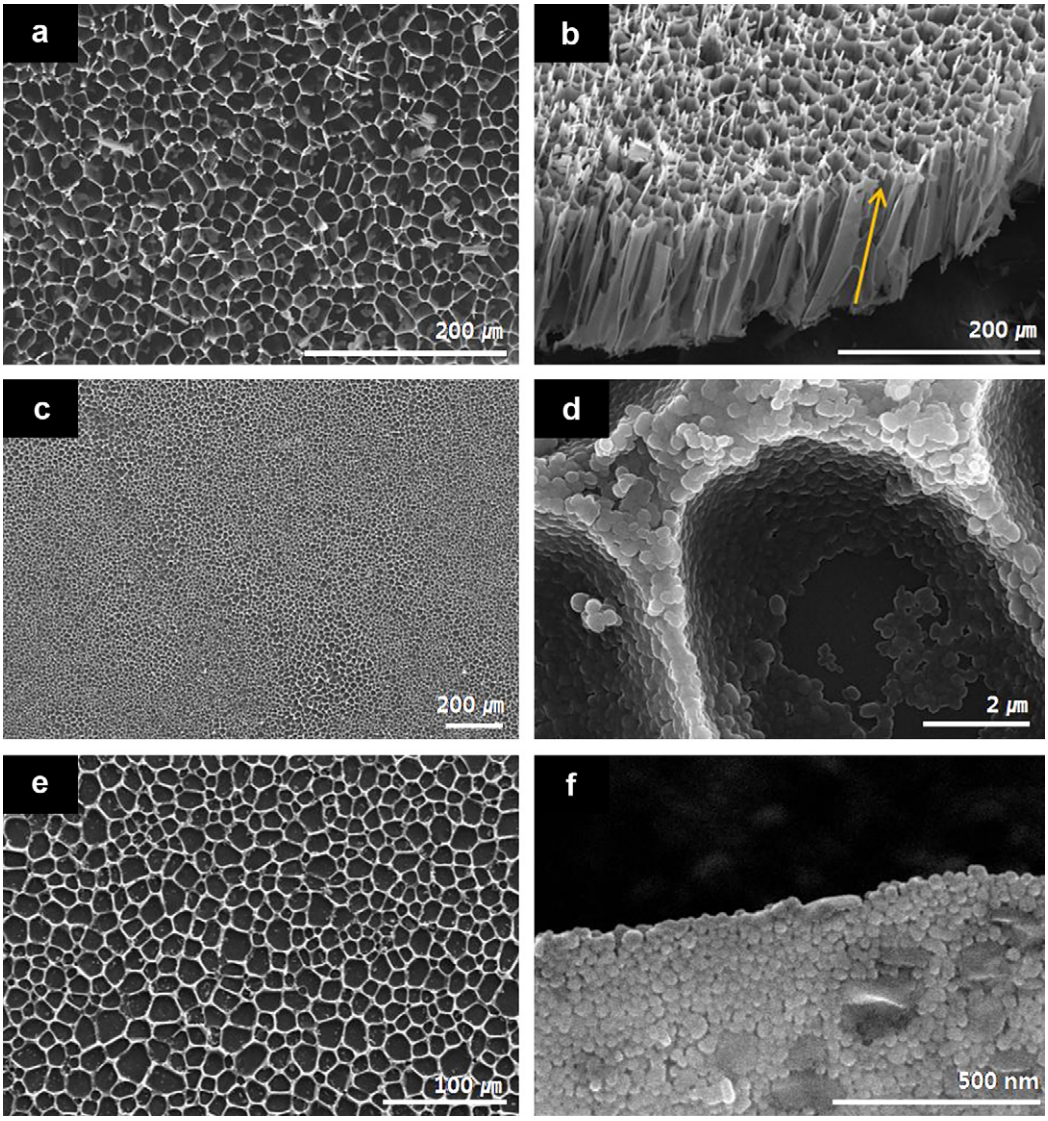

Fig. 2. Freeze-aligned porous networks of nanoparticles. Scanning electron microscopy (SEM) images of: (a) Cross section of aligned porous network of SiO_2 nanoparticles (20 nm, dispersion concentration: 5 wt%), (b) Vertical section of (a) along an alignment axis, (c) Aligned porous network of PTFE (200 nm, dispersion concentration: 30 wt%) nanoparticles showing long-range alignment, (d) PTFE nanoparticles making up porous networks at a higher magnification, (e) Aligned porous films of SiO_2/PTFE composite, and (f) Nanoparticulate structure of SiO_2/PTFE composite at a higher magnification.

SEM images in Fig. 2d reveal individual PTFE nanoparticles (200 nm) making up the wall of the porous PTFE networks (Fig. 2c). SEM image (Fig. 2d) showed nano-voids left between the nanoparticles that were remnants of water in the cryo-concentrate regions. The voids, indicating weak aggregation of the nanoparticles, inevitably made the whole structures mechanically weak, compared to the structures having continuous polymer walls.

An aligned porous structure of inorganic/organic (SiO_2/PTFE) nanoparticulate composites is shown in detail in Fig. 2e–f. The unidirectional freezing and subsequent freeze-drying process successfully produced the aligned through-thickness pore structure of SiO_2/PTFE. However, the case of mixed-dispersion with different components is more complicated than single-dispersion. This may be related to the different stabilities of colloidal SiO_2 and PTFE. The differences in particle sizes and chemical (or physical) nature lead to different mobilities of nanoparticles. Therefore, this situation may cause rather inhomogeneous pore size distribution (Fig. 2e). In the magnified image of Fig. 2f, both PTFE and smaller SiO_2 particles are visible. The voids between particles were smaller, compared to the PTFE case shown in Fig. 2d, but the network structure was still too weak to be a free-standing film. Other nanoparticles, such as TiO_2 and PSS–PEDOT, were processed into aligned porous films with similar pore morphology in a similar way (data not shown).

The size of pores could be modified by the dispersion concentration. Smaller pore sizes were observed over the entire sample at higher concentrations (Fig. 3). The higher concentration of nanoparticles restricted the growth of ice crystals and promoted more nucleation. Diffusion of nanoparticles ahead of the freezing front was significantly restricted, resulting in finer dendritic structures on the freezing front and smaller pores.

The pore size corresponded to the size of the columnar ice crystals before sublimation. Although the sublimation process could potentially induce the shrinking and collapsing of network structures, the difference between the size of the pores and the ice crystals was too small to notice in these experiments. Typical plots of ice crystal size as a function of experimental freezing rate (sample moving speed) and dispersion concentration are shown in Fig. 4. The average pore size increased as the freezing rate decreased, because the faster freezing rate created smaller ice crystals due to the greater amount of nuclei and limited time for ice crystal growth. A similar result was also obtained in the analysis of PSS–PEDOT nanoparticle cases.

We also compared the effects of dispersion concentration and freezing rate. An order of magnitude increase in freezing rate produced a similar order of magnitude decrease in the size of ice crystals, while an order of magnitude increase in dispersion concentration resulted in only a four-fold decrease in pore size. Accordingly, the freezing rate seems to be a more effective processing variable for controlling pore size.

As shown in Figs. 3 and 4, the pore size depended on the type of nanoparticles. For 30 wt% PTFE, the pore size was ca. 12.5 μm, while, for 30 wt% SiO_2, the pore size was ca. 3 μm (both 100 μm/s freezing rate). Even considering the volume fractions of PTFE and SiO_2 (density = 2.16 and 2.20 g/cm^3, respectively), the pore size significantly depended on the type of material. There are several reasons why different particles yield different pore sizes. First, particles of different sizes and types will induce different instability wavelengths in the ice front. Second, particle–particle interactions may cause aggregates. Third, large differences in surface energy can cause different ice-nanoparticle segregation behavior [23]. It has been reported that even different surfaces can induce different ice crystal structures [24].

3.2. Free-standing films

The resulting porous networks of colloidal nanoparticle systems were easily broken into fragments and particles, since the entire networks were too weakly connected to transfer stress. The networks were formed via the aggregation of nanoparticles by ice-induced segregation. This physical aggregation was not strong

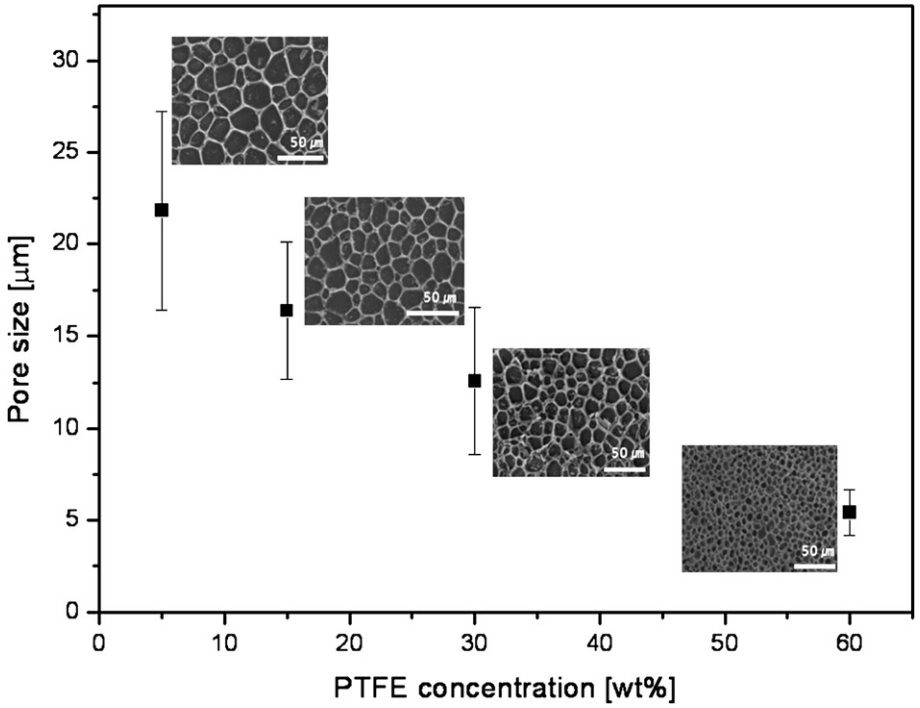

Fig. 3. Control of pore size by varying dispersion concentration. Average size of aligned pores vs. dispersion concentration of PTFE nanoparticles in water. The SEM micrographs show aligned PTFE networks of different concentrations after drying. Scale bar = 50 μm.

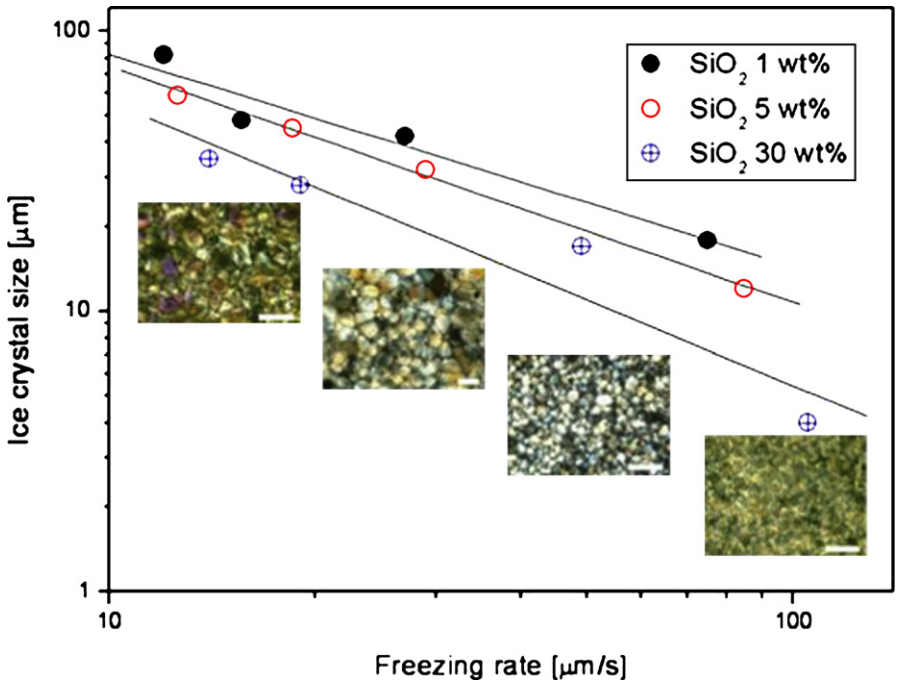

Fig. 4. Controlling the porous network structure: ice crystal diameter vs. freezing rate. The optical micrographs show aligned SiO_2 networks before drying frozen at different sample moving speeds (freezing rate). Scale bar = 100 μm.

enough to maintain the entire network coherently. Aligned porous networks of colloidal systems are difficult to handle because of their brittleness. We tried various approaches to resolve this drawback and develop this method for the preparation of useful free-standing porous material membranes.

First, we produced porous networks of inorganic/organic composites by the unidirectional freezing method. Mixed solutions of dissolved polymers and dispersed SiO_2 nanoparticles were directionally frozen and freeze-dried to produce the porous inorganic/polymer composite materials shown in Fig. 5. SiO_2/PVDF composite (Fig. 5a–c) and SiO_2/HPC composite (Fig. 5d and e) were investigated to prepare mechanically strong films of 100–150 μm thickness. Freezing excluded the polymer chains and SiO_2 nanoparticles from the freezing front of the growing ice crystals, and the polymer chains and nanoparticles were aggregated and assembled into a cryo-concentrate phase. When significant chain entanglements occur, a mechanically strong composite phase can result. The polymer in the continuous phase plays a vital role as a structuring

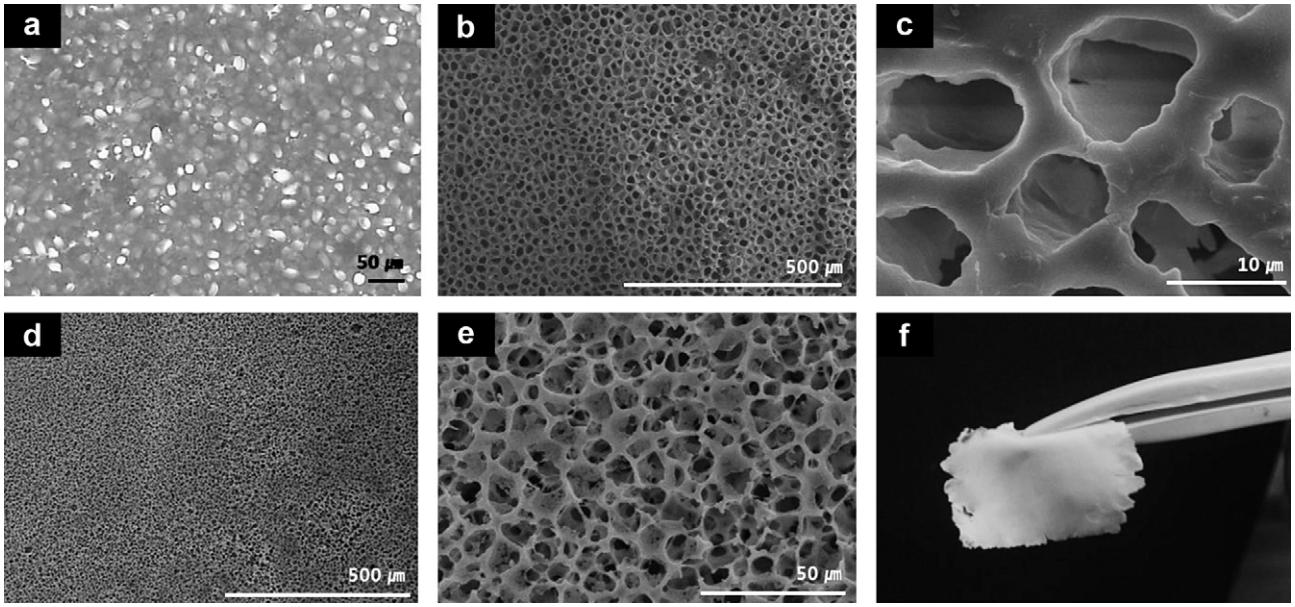

Fig. 5. Porous networks of inorganic/polymer composites. (a) OM image (transmission mode) of SiO_2/PVDF composite, (b) SEM images of cross section of porous network of SiO_2/PVDF composite, (c) SiO_2/PVDF composite at a higher magnification, (d) SEM image of cross section of SiO_2/HPC composite, (e) SiO_2/HPC composite at a higher magnification, and (f) Photographic image of a free-standing SiO_2/HPC composite film that could be easily handled with tweezers.

agent in these materials despite being the minor component in the composites. After proper freeze-drying, a free-standing inorganic/polymer composite film of 100–150 μm thickness, which could be handled with tweezers, was obtained (Fig. 5f). HPC, a typical binder for ceramic materials, also produced a similar free-standing membrane. In magnified images like Fig. 5c, the composite materials showed improved connectivity of materials and no evidence of individual particles. Additionally, the SiO_2/PVDF sample has more cellular structures, while the SiO2/HPC sample has more fibrillar structures, possibly due to the difference in the instability formation by diffusion.

Second, we used the phase structures of emulsions to tune pore morphologies over a wide range, making it possible to control the physical properties of porous networks. In this approach, the SiO_2 water phase was emulsified in cyclohexanone, and both the cyclohexanone (T_m −16.4 °C) and water phases were frozen and removed by freeze-drying. Through this controlled freezing of an emulsion, a multi-scale porous network with a complex pore structure was prepared (Fig. 6a and b). The porous SiO_2–PVDF composite showed weakly aligned and rather poorly connected pore structures (Fig. 6a) with some pores of a few microns and the others of submicrons. The micron and submicron pores reflected the spaces occupied by the crystals of cyclohexanone (continuous phase containing PVDF) and water (aqueous phase containing SiO_2 nanoparticles), respectively.

During freezing of water-in-oil emulsions, the water minor phase freezes first, and then the freezing of cyclohexanone excludes SiO_2 nanoparticles, ice submicron particles, and PVDF polymer chains. The excluding behaviors of the three different materials are different, resulting in a relatively strong cryo-concentrate phase of the complex structure. Due to the low mobility of supporting polymer matrix and particles, the growth of columnar solvent crystals will be restricted, resulting in high tortuosity.

The stability of the aqueous phase may be controlled by PVDF molecular chains in the continuous phase. The repulsive forces between water droplets [25] by the chain entanglement of PVDF in the continuous phase could be sufficient to limit droplet aggregation. The emulsion can also be stabilized by SiO_2 nanoparticles adsorbed onto the interface between cyclohexanone and water (Pickering emulsion) [26,27]. As freezing progresses, the structures in the liquid state will be partially destroyed depending on the nucleation and growth process of crystals. However, the pore morphology in Fig. 6 shows that the structure in the liquid state remained to a certain extent even after freeze-drying. The resulting networks had improved connectivity, which strengthened the porous films. Third, we tried the post-annealing of nanoparticulate networks. The driving force of thermal annealing (sintering) [28] is the minimization of surface free energy, brought about from a gradient in the chemical potential. During this process, nanoparticles find a more stable configuration by decreasing their surface area [29]. SEM images of the surface structures of the aligned networks before and after annealing are shown in Fig. 7. After thermal annealing, individual SiO_2 nanoparticles were difficult to observe, and related surface area reduction was noticed in the aligned porous SiO_2 network (Fig. 7a and b). The pore structures observed in a low magnification were not significantly changed by the annealing process (similar to Fig. 2).

We also tried solvent annealing for PTFE nanoparticulate networks under saturated HF solvent vapor. The samples were placed in a chamber, i.e., an upside-down Teflon container having saturated HF vapor. To maintain the condition of saturated HF vapor, the chamber was covered by a larger Teflon container. The samples were annealed for at least 4 h, and the upside-down Teflon container was then simply removed, thus allowing the HF in the swollen PTFE networks to evaporate. This controlled annealing process improved the mobility of PTFE molecular chains. The surface morphology of the networks was dependent on the annealing time. At a relatively short annealing time (1–2 h), the network surface showed no changes. When the annealing time exceeded 24 h, inhomogeneity in the porous structures was observed, which might be related to collapsed and disordered networks. Annealing of 4–24 h improved the mobility of PTFE molecular chains, accompanied by particle fusion caused by surface free energy. The surface images of the PTFE networks before and after solvent annealing show the changed connectivity in the particulate networks (Fig. 7c and d). The detailed bulk mechanical properties, such as the modulus and toughness, are currently under investigation.

3.3. Surface characterization

AFM was applied to measure the surface mechanical behavior of porous networks. The interaction force between the tip and the sample is affected by the surface structure (contact area), the materials that the tip and the sample are made of, and environmental conditions, such as temperature and humidity [30]. Accordingly, all of the experimental conditions were kept constant during this measurement in order to focus on the effect of the materials. In addition, the adhesion force is dependent on capillary forces between a tip and a sample surface [31], and so we maintained a stable capillary force through humidity control.

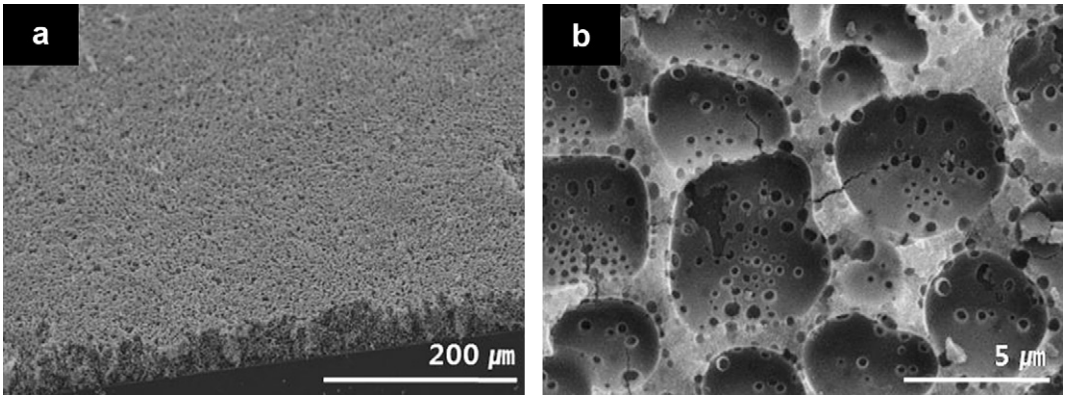

Fig. 6. Aligned porous networks created by the controlled freezing of emulsion. (a) Vertical sectional SEM image showing long-range ordering and (b) Cross section of aligned porous SiO_2/PVDF composites with a continuous oil phase and minor water droplet phase.

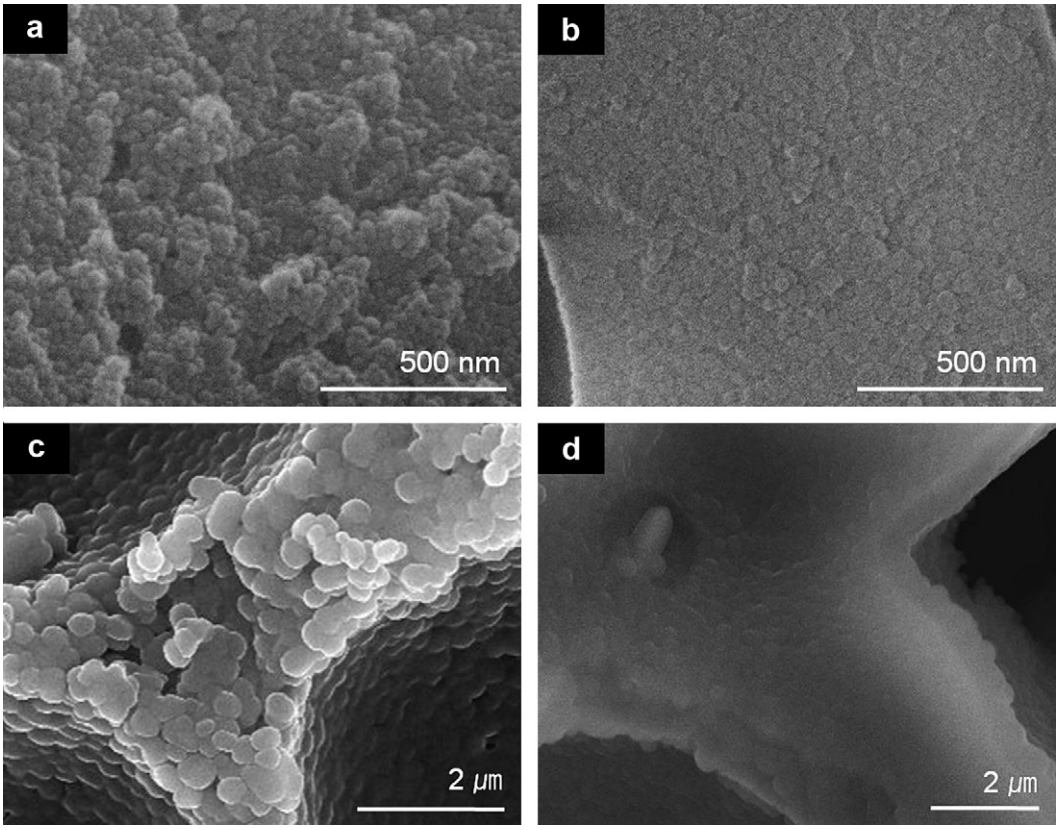

Fig. 7. Improved connectivity of aligned porous networks by post-annealing. SEM images of: (a) Surface of the aligned porous SiO_2 network shown in Fig. 1(a and b) Surface of the SiO_2 network showing surface area reduction after thermal annealing at 600 °C for 5 h (2 °C/min), (c) Surface of the aligned porous PTFE network shown in Fig. 1(c) and (d) Surface of the solvent-annealed PTFE network (under saturated HF solvent vapor for 4 h).

The representative approach and retrace F-D curve of AFM force measurement is shown in Fig. 8a. As a surface property, the adhesion force between the AFM tip and the surface of the networks was investigated. The retrace part of the inset curve in Fig. 8a shows adhesion characteristics. Faster freezing rates made smaller adhesion forces. The surface content of PTFE significantly influenced the adhesion property. The decrease in adhesion force with an increase in freezing rate seemed to indicate an increase in PTFE content on the surface.

The top surface of porous networks contains materials excluded from the growing ice crystal phases at the last stage of freezing. The composition of the liquid phase at the last stage determines the adhesion property (Fig. 8a). As the ice columnar phase grows, the remaining liquid phase has less and less water content, which could change the concentrations of SiO_2 and PTFE. Faster freezing could result in a higher concentration of PTFE in the liquid phase at the last stage of freezing. The exclusion processes of PTFE and SiO_2 may not be the same, possibly because of differences in size or surface free energy. According to our theoretical approach, which will be discussed later, the engulfing of particles by the ice phase should be more prominent in cases of smaller particles (SiO_2 in this case, thus more PVDF on the surface). Indeed, our recent study on FT-IR 2D mapping showed that the composition of cryo-concentrated regions was quite inhomogeneous, as the fluctuation in local concentration was significant (data not shown).

The approach part reveals how the network deforms upon the impact of a tip. The slope of this curve reflects surface hardness. The values of the slope for different samples are given in Fig. 8b. The average hardness value of the solvent-annealed PTFE network was similar to that of PTFE prepared without annealing. The annealing procedure had a negligible effect on the hardness property of the top surface of a few nanometers, which is the space usually probed by an AFM tip. It did have a decisive effect on the connectivity of the nanoparticles in a larger scale, allowing us to produce free-standing membranes (Fig. 7).

The enhanced surface hardness of networks on a nano scale was observed when we added inorganic nanoparticles. The hardness of the composites increased with increasing SiO_2 content (Fig. 8b). The SiO_2 nanoparticles (20 nm) acted as inorganic fillers, which closely packed with PTFE nanoparticles (200 nm) and resulted in a reduced void content. The SiO_2 nanoparticles seemed to carry significant mechanical stress. The presence of nano-voids in the networks obviously deteriorates their mechanical properties [32,33].

Representative contact-mode AFM images of particulate networks are shown in Fig. 8b. PTFE nanoparticles are visible in all the images. When SiO_2 nanoparticles were added, the smaller SiO_2 particles were visible. Fig. 8b indeed shows the different surface morphology in the case of a 1/1 wt ratio (SiO_2/PTFE). The surface roughness does not appear to dominantly affect the indentation hardness trend in Fig. 8b, since the apparent roughness in the AFM images did not match the hardness trend, although more detailed analysis is required to confirm the effect of surface roughness.

4. Discussion

Dissolved polymer chains, inorganic, and organic nanoparticles tend to be excluded from the ice phase during freezing, since the solubility of a solute in ice is almost negligible. As freezing rate

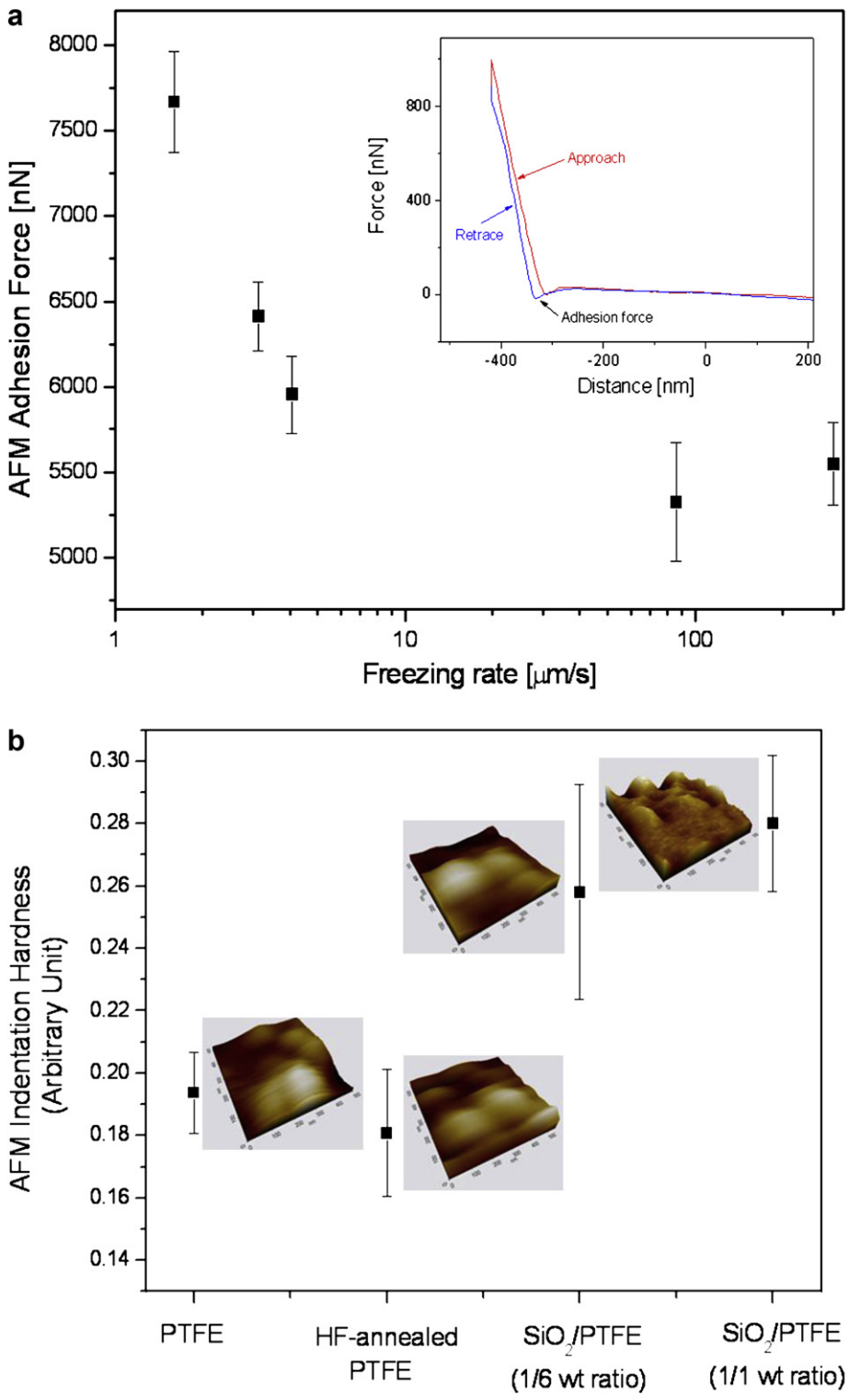

Fig. 8. Nanoscopic properties of freeze-aligned porous networks probed by AFM. (a) Adhesion force between the AFM tip and surface of aligned SiO_2/PTFE composites. The inset shows the typical force–distance curve of AFM measurement. (b) AFM indentation hardness of four different samples and their representative contact-mode AFM images (500 × 500 nm).

increases, however, the nanoparticles or polymer-rich phases can be engulfed by the ice phase. If there is no interaction among particles (obviously an oversimplification), simple theoretical principles can be developed for flat interfaces. For a particle to be rejected by the ice phase, the surface free energy at a minimum separation, $\Delta\sigma = \sigma_{sp} - (\sigma_{lp} + \sigma_{sl})$, should be positive, where σ_{sp}, σ_{lp}, and σ_{sl} are the interfacial free energies of solid-particle, liquid-particle, and solid–liquid interfaces, respectively. The specific interactions among ice, water, and nanoparticles are important for fabricating ice-templated structures. By combining the equation

with the mass balance and diffusion equations, the critical velocity below which particles will be excluded, v_c, is

$$v_c = \frac{\nabla\sigma d}{3\eta r}\left(\frac{a_o}{d}\right)^n \quad (1)$$

where d is the distance between the particle and the interface (freezing front), η is viscosity of water, r is the radius of the particle, a_o is the intermolecular distance of water, and n is an exponent that is larger than 1. This simple equation provides a basic understanding of the effects of influencing factors, such as particle size [4,6,34].

The typical freezing rate used in this experiment seems to be far below the critical velocity, which is typically 1–0.1 m/s [6]. In fact, the well developed columnar structure of the ice phase that we have observed so far supports this conjecture. However, particle engulfing could occur even below the critical velocity, since the analysis did not consider interparticulate interactions. Once particles (or polymer chains) accumulate at the front of the interface, the mobility of particles (or polymer chains) will dramatically decrease, resulting in engulfing particle or polymer-rich phases. The restricted growth of ice columns depicted in Fig. 5, which shows ramified columnar structures, might be due to this reason.

The flat interface of the freezing front excludes solutes and develops a significant concentration gradient. The overall freezing rate is determined by the rate of heat extraction, and the local growth rate is limited by the low liquid diffusivity. Therefore, above a certain freezing rate, the flat freezing front adapts to a dendritic shape, which then becomes columnar or lamellar structures later. The formation of columnar structures is known as Mullins–Sekerka instability [35]. Kurz and Fischer suggested that dendrite morphology is defined by sinusoidal perturbations at the solid–liquid interface. There exists a threshold wavelength that leads to the formation of stable dendrites; below this wavelength, the perturbations disappear. This limit is known as the limit of morphological stability and is used to define the crystal size in relation to freezing kinetics [36]. Simple particle pinning can cause the same dendrites [5,6].

As ice crystals grow, there is a rejection of nanoparticles and heat from the moving interface into the remaining unfrozen solvent that causes supersaturation and supercooling to occur. As heat transfer rates are normally much greater than mass transfer rates, nanoparticle diffusion tends to control the growth of the ice crystals. On the basis of Fick's law and materials balance, theoretical equations to describe the intercolumnar spacing in the case of very dilute solutions have been proposed. Rohatgi and Adams [23] proposed the following spacing between the dendrites (columns), L,

$$L = (8D\Delta T)^{0.5}F^{-0.5} \quad (2)$$

where D is the binary diffusion coefficient related to the concentration term, ΔT is the supercooling between dendrites, and F represents the freezing rate. They proved that the supersaturation and supercooling are independent of freezing rate, and their experimental results proved the relationship between L and D or F.

Although the above equation does not consider the interactions between particles, particle size distribution, viscoelastic properties of slurry, latent heat diffusion, or partial solidification in cryo-concentrated regions, among others, the equation provides a successful qualitative explanation of the ice crystal size (pore size) in our experiments. As the concentration of SiO_2 (or PTFE) nanoparticles increases, D decreases and L will decrease also (Figs. 3 and 4). The effect of freezing rate also follows the equation, since an increase in F is followed by a decrease in L (Fig. 4). The slopes of Fig. 4 are smaller than −0.5, but still quite close, although the freezing rate used in our experiment was purely experimental (strictly speaking, not F in eqn (2)).

When we used SiO_2 and PTFE particles, the resulting pore size seemed to qualitatively follow the above equation. When we added a small amount of polymer chains dissolved in a mixed solvent, the pore morphology became different, showing that the ice columns seemed to be ramified during their longitudinal growth (Fig. 5). The existence of polymer chains and mixed solvents, in addition to the nanoparticles, restricted solute diffusion and the longitudinal growth of ice crystals. The use of emulsion and subsequent annealing further changed the morphology of the pores.

The use of composite materials of inorganic nanoparticles (SiO_2) and polymers (PVDF), and subsequent annealing, represents a promising process to create through-thickness pores and relatively strong mechanical properties.

5. Conclusion

PTFE and PVDF porous membranes are widely used in various applications. Using a unidirectional method of freezing nanoparticles, through-thickness porous structures were successfully fabricated from PVDF and PTFE. The nanoparticles aggregated in the cryo-concentrate phases between the growing columnar ice crystals under properly controlled freezing conditions. By varying the dispersion concentration between 5 and 60 wt% and the freezing rate between 100 and 200 μm/s, pore size could be adjusted in the range of 2–60 μm. To overcome the drawbacks of the brittle, weakly connected nanoparticulate structures prepared by the unidirectional freezing process, inorganic/polymer composite networks were fabricated. As a result, free-standing membranes with improved mechanical properties were prepared. Additional post-annealing procedures can further improve the coherence of a particulate material. The underlying mechanism can be qualitatively explained by the simple principles of dendritic freezing fronts of water containing solutes and/or particles. This simple environmentally friendly process has potential applications and offers a high level of control over the properties of various porous materials.

Acknowledgements

This research was supported by a grant from the Fundamental R&D Program for Core Technology of Materials (Ministry of Knowledge Economy) and the Ministry of Health and Welfare in South Korea (A090996). M.K.L. would like to thank the Human Resource Training Project for Strategic Technology (MKE and KOTEF).

References

[1] Spoerke ED, Murray NGD, Li H, Brinson LC, Dunand DC, Stupp SI. J Biomed Mater Res A 2008;84A:402.
[2] Yamaguchi A, Uejo F, Yoda T, Uchida T, Tanamura Y, Yamashita T, et al. Nat Mater 2004;3:337.
[3] Vallet-Regí M, Balas F, Arcos D. Angew Chem Int Ed 2007;46:7548.
[4] Colard CAL, Cave RA, Grossiord N, Covington JA, Bon SAF. Adv Mater 2009;21:2894.
[5] Deville S, Saiz E, Nalla RK, Tomsia AP. Science 2006;311:515.
[6] Deville S, Saiz E, Tomsia AP. Acta Materialia 1965;2007:55.
[7] Zhang H, Edgar D, Murray P, Rak-Raszewska A, Glennon-Alty L, Cooper AI. Adv Funct Mater 2008;18:222.
[8] Zhang H, Cooper AI. Adv Mater 2007;19:1529.
[9] Zhang H, Lee JY, Ahmed A, Hussain I, Cooper AI. Angew Chem 2008;47:4573.
[10] Zhang H, Hussain I, Brust M, Butler MF, Rannard SP, Copper AI. Nat Mater 2005;4:787.
[11] Mukai SR, Nishihara H, Schichi S, Tamon H. Chem Mater 2004;16:4987.
[12] Gutierrez MC, Jobbagy M, Rapun N, Ferrer ML, del Monte F. Adv Mater 2006;18:1137.

[13] Yunoki S, Ikoma T, Monkawa A, Ohta K, Kikuchi M, Sotome S, et al. Mater Lett 2006;60:999.
[14] Svagan AJ, Azizi Samir MAS, Berglund LA. Adv Mater 2008;20:1263.
[15] Pääkkö M, Vapaavuori J, Silvennoinen R, Kosonen H, Ankerfors M, Lindström T, et al. Soft Matter 2008;4:2492.
[16] Zeng C, Han X, Lee LJ, Koelling KW, Tomasko DL. Adv Mater 2003;15:1743.
[17] Lee LJ, Zeng C, Cao X, Han X, Shen J, Xu G. Compos Sci Technol 2005;65:2344.
[18] Lee J, Cheng Y. J Controlled Release 2006;111:185.
[19] Lee MK, Kim MY, Kim S, Lee J. J Pharm Sci 2009;98:4808.
[20] Tortonese M, Kirk M. Int Soc Opt Eng 1997;3009:53.
[21] Lee J. Macromol Biosci 2005;5:1085.
[22] Lee J. Int J Pharm 2007;340:191.
[23] Rohatgi PK, Adams CM. Trans Metallurg Soc AIME 1967;239:1729.
[24] Ehre D, Lavert E, Lahav M, Lubomirsky I. Science 2010;327:672.
[25] Derjaguin BV. Langmuir 1987;3:601.
[26] Aveyard R, Binks BP, Clint JH. Adv Colloid Interface Sci 2003;100-102:503.
[27] Binks BP. Curr Opin Colloid Interface Sci 2002;7:21.
[28] Sleptsov VM, Shcherbina OD, Trunov GV. Poroshk Metall 1975;7:99.
[29] Dutta J, Hofmann H, Houriet R, Hofmeister H, Hollenstein C. Colloids and Surfaces A Physicochemical and Engineering Aspects 1997;127:263.
[30] Burnham NA, Dominguez DD, Mowery RL, Colton RJ. Phys Rev Lett 1931;1990:64.
[31] Burnham NA, Colton RJ, Pollock HM. Nanotechnology 1993;4:64.
[32] Hussain M, Oku Y, Nakahira A, Niihara K. Mater Lett 1996;26:177.
[33] Wetzel B, Haupert F, Zhang MQ. Compos Sci Technol 2003;63:2055.
[34] Uhlmann DR, Chalmers B, Jackson KA. J Appl Phys 1964;35:2986.
[35] Hadji L. Eur Phys J B 2004;37:85.
[36] Kurz W, Fisher DJ. Acta Metallurgica 1981;29:11.